# Vibration of Tensioned Beams with Intermediate Damper. I: Formulation, Influence of Damper Location

Joseph A. Main, A.M.ASCE[1], Nicholas P. Jones, M.ASCE[2]

**Abstract:** Exact analytical solutions are formulated for free vibrations of tensioned beams with an intermediate viscous damper. The dynamic stiffness method is used in the problem formulation, and characteristic equations are obtained for both clamped and pinned supports. The complex eigenfrequencies form loci in the complex plane that originate at the undamped eigenfrequencies and terminate at the eigenfrequencies of the fully locked system, in which the damper acts as an intermediate pin support. The fully locked eigenfrequencies exhibit "curve veering", in which adjacent eigenfrequencies approach and then veer apart as the damper passes a node of an undamped mode shape. Consideration of the evolution of the eigenfrequency loci with varying damper location reveals three distinct regimes of behavior, which prevail from the taut-string limit to the case of a beam without tension. The second regime corresponds to damper locations near the first anti-node of a given undamped mode shape; in this regime the loci bend backwards to intersect the imaginary axis, and two distinct non-oscillatory decaying solutions emerge when the damper coefficient exceeds a critical value.

**CE Database subject headings:** Vibration; Damping; Modal Analysis; Eigenvalues; Beams; Cables; Tensile members.

## Introduction

Supplemental dampers are finding increased application for vibration suppression in structures (e.g., Rasmussen 1997), and practical considerations often dictate that dampers be incorporated at a few specific locations rather than being distributed throughout the structure. Problematic cable vibrations in cable-stayed bridges, for example, have been successfully mitigated by attaching a single damper to each cable transversely near the anchorage (e.g., Main and Jones 2001). Such concentrated forms of damping are inherently non-classical when applied to a continuous system such as a cable or beam,

[1] Research Structural Engineer, National Institute of Standards and Technology, 100 Bureau Drive, Stop 8611, Gaithersburg, MD 20899. joseph.main@nist.gov
[2] Professor and Dean, Whiting School of Engineering, Johns Hopkins University, 3400 N. Charles Street, Baltimore, MD 21218. npjones@jhu.edu

and because supplemental dampers can be designed to produce large forces, dampers have the potential to significantly modify the mode shapes of a system as well as providing dissipation. The resulting mode shapes are complex-valued, representing oscillations that vary in phase throughout the system. Such modifications of the mode shapes are of fundamental importance in effective design of supplemental dampers, because if a damper is too strong, it can "lock" the system locally, perturbing the mode shapes and shifting the eigenfrequencies but providing negligible dissipation. An optimal damper tuning generally exists, for which the maximum damping efficiency is achieved in a particular mode of vibration.

While the complex modes of a continuous system can be approximated using a finite series of undamped mode shapes, a large number of terms may be required to achieve adequate convergence in cases of concentrated damping. For example, in studying the vibrations of a taut string with a viscous damper attached near one end, Pacheco et al. (1993) found that more than 200 undamped mode shapes were required for convergence of the first-mode damping ratio. Alternatively, the complex modes can be evaluated exactly by direct solution of the governing partial differential equations including the concentrated damping forces. Such exact solutions generally lead to characteristic equations involving transcendental functions, from which the complex eigenfrequencies are evaluated numerically. Several previous studies have developed analytical solutions for the complex modes of specific continuous systems with concentrated damping. McBride (1943) evaluated the complex modes for both lateral and longitudinal vibrations of a cantilever beam with a terminal dashpot, and the case of longitudinal vibrations was revisited by Singh et al. (1989) and Hull (1994). Lateral

vibrations of a beam with rotational viscous dampers at the ends were considered by Oliveto et al. (1997) and Krenk (2004). While these studies considered damping at the boundaries, several recent studies have considered concentrated damping at an intermediate point. The taut string with intermediate damper, investigated numerically by Pacheco et al. (1993), was revisited using an analytical solution for the complex modes by Krenk (2000) and Main and Jones (2002), and Krenk and Nielsen (2002) considered a sagging cable with intermediate damper. Krenk (2004) recently developed a general state-space formulation for complex modal analysis of continuous systems, analogous to the well-established approach for discrete systems (Foss 1958), whereby orthogonality relations for the complex modes can be used to express the response to arbitrary forcing as a superposition of uncoupled responses in the complex modes.

In this paper, exact analytical solutions are developed for the complex modes of lateral vibration for a uniform axially loaded beam with an intermediate viscous damper for both clamped and pinned support conditions, as depicted in Fig. 1. These solutions are developed using a dynamic stiffness formulation, to facilitate treatment of different boundary conditions and to enable the present formulation to be readily extended to more complicated assemblages. These results are of fairly broad relevance, because the axially loaded beam can represent a wide class of structural elements, reducing to a standard Bernoulli beam for zero axial load and to a taut string in the limit of zero bending stiffness. The relative importance of axial loading and bending stiffness is represented through the nondimensional parameter $\gamma$, as defined by Irvine (1981):

$$\gamma = \sqrt{\frac{Tl_0^2}{EI}} \tag{1}$$

where $T$ = axial tension, $l_0$ = total span length, $E$ = elastic modulus, and $I$ = moment of inertia. The limit $\gamma \to \infty$ corresponds to a taut string, while $\gamma = 0$ corresponds to a beam without axial load. As discussed by Cole (1968), when $\gamma$ becomes large, the system exhibits "boundary layers", or local regions in which the influence of bending stiffness is important in satisfying boundary conditions or discontinuities; outside of these regions, bending stiffness has only a small influence on the solution. The existence of such boundary layers can present a challenge for discretization schemes such as the finite element method, potentially requiring a high degree of spatial refinement to accurately represent the solution characteristics. A number of previous studies have developed analytical solutions for the eigenfrequencies and mode shapes of single-span tensioned beams under various end conditions (e.g., Seebeck 1852, Wittrick 1986, Bokaian 1990, Liu et al. 1996), and Currie and Cleghorn (1988) considered a tensioned beam with a concentrated mass at midspan. Formulations using Green's functions (Bergman and Hyatt 1989) and transfer matrices (Franklin 1989) have also been developed to analyze the free vibrations of axially loaded beams with pin supports, springs, masses, and oscillators attached at intermediate locations.

In this paper, characteristic equations are obtained for the systems in Figs. 1(a) and 1(b), and these equations are expressed in a relatively simple form in terms of factors associated with cases of single-span vibration. Examination of the solution characteristics reveals a number of complicated and non-intuitive features resulting from the non-classical nature of the damping. The eigenfrequencies are observed to form loci in the complex plane that originate at the real-valued undamped eigenfrequencies and terminate at the eigenfrequencies of the fully locked system, in which the damper acts as an

intermediate pin support. These eigenfrequency loci are analogous to the root locus plots commonly considered in the design of active control systems (e.g., Preumont 2002). The eigenfrequencies of the fully locked system are found to exhibit a "curve veering" phenomenon (e.g., Perkins and Mote 1986), in which adjacent eigenfrequencies approach and then veer apart as the damper passes the node of an undamped mode shape.

The evolution of the eigenfrequency loci with varying damper location is considered, and three distinct regimes are observed for damper locations between the support and the first node of a given undamped mode shape. These regimes correspond to those described by Main and Jones (2002) for the taut string with viscous damper, and it is observed that the general features of these regimes persist for all values of $\gamma$, from the taut-string limit to the case of a beam without tension. Interestingly, when the damper is located sufficiently near the first anti-node of a particular mode, the eigenfrequency locus associated with that mode bends backwards to intersect the imaginary axis, and two distinct non-oscillatory solutions emerge when the damper coefficient exceeds a critical value. It is thus observed that free oscillation in a particular mode can be completely suppressed by appropriate placement and tuning of the damper. The present solution is of particular relevance for stay-cable vibration suppression, as discussed in the companion paper (Main and Jones 2005), which presents efficient iterative and asymptotic solutions for the complex eigenfrequencies and investigates the solution characteristics for cases in which the damper is relatively near a support.

## Problem Formulation

Free lateral vibrations are considered for a uniform axially loaded beam with intermediate viscous damper for both clamped and pinned support conditions, as depicted in Fig. 1. The linear viscous damper with coefficient *c* is attached at an intermediate point, dividing the beam into two segments of length $l_1$ and $l_2$. Because the supports are symmetric in both cases under consideration, it can be assumed without loss of generality that $l_1 \le l_2$. The dynamic stiffness matrix is first obtained for a general segment of tensioned beam with length $l_j$, where the subscript $j$ denotes the segment index, and the dynamic stiffness contributions from the two segments on each side of the damper are then assembled into global dynamic stiffness matrices for the cases of clamped and pinned supports. Characteristic equations for determination of the complex eigenfrequencies are obtained from the determinants of these matrices.

### *Dynamic Stiffness Matrix and Frequency-Dependent Shape Functions*

The dynamic stiffness matrix is obtained for a segment of tensioned beam with length $l_j$, as shown in Fig. 2. The coefficients of the dynamic stiffness matrix relate the oscillatory end displacements and rotations, shown in Fig. 2(b), to the oscillatory end shear forces and bending moments, shown in Fig. 2(a). The time variation of these quantities is represented through the complex exponential $e^{i\omega t}$, where $i = \sqrt{-1}$, with the implicit understanding that the physical displacements and forces are represented by the real parts. When applied to free vibrations with dissipation, the frequency $\omega$ is generally complex-valued, with its real part giving the frequency of damped oscillation and its

imaginary part giving the rate of decay. The displacement and force coefficients (e.g., $\alpha_a$ and $V_a$) are also complex-valued in general to allow for arbitrary phasing among the end forces and displacements. It is convenient to introduce the following alternative nondimensional versions of $\omega$:

$$\hat{\omega} = \omega / \omega_{01}^{S};\ \tilde{\omega} = \omega / \omega_{01}^{B} \tag{2}$$

where $\omega_{01}^{S} = \pi / l_0 \sqrt{T/m}$ is the fundamental frequency of a taut string, and $\omega_{01}^{B} = \pi^2 / l_0^2 \sqrt{EI/m}$ is the fundamental frequency of a beam with pinned supports. The caret is used to denote the "taut-string" nondimensionalization $\hat{\omega}$, suitable for large $\gamma$, with its kink symbolizing the fact that concentrated forces produce discontinuities in slope in the absence of flexural stiffness, and the tilde is used to denote the "beam" nondimensionalization $\tilde{\omega}$, suitable for small $\gamma$, with its curvature symbolizing that nonzero flexural stiffness requires the slope to be continuous. The two are related by $\tilde{\omega} = \gamma \hat{\omega} / \pi$, where $\gamma$ is the nondimensional parameter defined in Eq. (1).

With no loading along the span, the equation of motion for each segment is then given by the following well-known partial differential equation, assuming small deflections in a single plane and neglecting shear deformation, rotary inertia, and internal damping:

$$EI \frac{\partial^4 y}{\partial x_j^4} - T \frac{\partial^2 y}{\partial x_j^2} + m \frac{\partial^2 y}{\partial t^2} = 0 \tag{3}$$

where $y(x_j, t)$ = transverse deflection and $x_j$ = axial coordinate along the $j^{th}$ segment. Eq. (3) represents a balance of the inertial force with the derivative of the shear force

$V(x_j,t)$ on a vertical section of the tensioned beam, and the shear force $V(x_j,t)$ and bending moment $M(x_j,t)$ are given by

$$V(x_j,t) = EI\frac{\partial^3 y}{\partial x_j^3} - T\frac{\partial y}{\partial x_j};\ M(x_j,t) = EI\frac{\partial^2 y}{\partial x_j^2} \tag{4}$$

Accounting for differences in sign conventions, the end forces and moments, shown in Fig. 2(a), can be expressed in terms of the internal shear force and bending moments, defined in Eq. (4), as follows:

$$V(0,t) = V_a e^{i\omega t};\ -V(l_j,t) = V_b e^{i\omega t} \tag{5}$$

$$-M(0,t) = M_a e^{i\omega t};\ M(l_j,t) = M_b e^{i\omega t} \tag{6}$$

The solution to the partial differential Eq. (3) subject to the boundary conditions in Eqs. (5) and (6) can be represented in the following form:

$$y(x_j,t) = Y(x_j)e^{i\omega t} \tag{7}$$

Substituting Eq. (7) into Eq. (3) yields a fourth-order ordinary differential equation for $Y(x_j)$. While the resulting solution for $Y(x_j)$ has often been expressed using a combination of hyperbolic and trigonometric functions, Tang (2003) points out that the use of hyperbolic functions can lead to numerical difficulties when using finite-precision arithmetic. Tang's study considered a beam without tension, and such numerical difficulties are exacerbated by the presence of axial tension, as discussed by Franklin (1989). Improved numerical conditioning is achieved by expressing the solution in the following equivalent form:

$$Y(\xi_j) = A_1 e^{-p\xi_j} + A_2 e^{-p(\mu_j - \xi_j)} + A_3\cos q\xi_j + A_4 \sin q\xi_j \tag{8}$$

in which the nondimensional axial coordinate $\xi_j = x_j / l_0$ and the nondimensional segment length $\mu_j = l_j / l_0$ have been introduced, and $p$ and $q$ can be expressed in terms of the alternative nondimensional frequencies as follows:

$$\left.\begin{matrix} p \\ q \end{matrix}\right\} = \sqrt{\sqrt{(\tfrac{1}{2}\gamma^2)^2 + (\pi\gamma\hat{\omega})^2} \pm \tfrac{1}{2}\gamma^2} = \sqrt{\sqrt{(\tfrac{1}{2}\gamma^2)^2 + (\pi^2\tilde{\omega})^2} \pm \tfrac{1}{2}\gamma^2} \tag{9}$$

The following relations follow directly from Eq. (9):

$$p^2 - q^2 = \gamma^2; \;\; pq = \pi^2\tilde{\omega} = \pi\gamma\hat{\omega} \tag{10}$$

In formulating the dynamic stiffness matrix, it is necessary to relate the end forces directly to the end displacements, eliminating the solution coefficients in Eq. (8). With rotations assumed sufficiently small that they can be approximated by the slopes, the end displacements depicted in Fig. 2(b) are related to the solution coefficients in Eq. (8) as follows:

$$\begin{Bmatrix} Y(0) \\ Y'(0) \\ Y(\mu_j) \\ Y'(\mu_j) \end{Bmatrix} = \begin{Bmatrix} \alpha_a \\ \theta_a l_0 \\ \alpha_b \\ \theta_b l_0 \end{Bmatrix} = \begin{bmatrix} 1 & \varepsilon_j & 1 & 0 \\ -p & p\varepsilon_j & 0 & q \\ \varepsilon_j & 1 & C_j & S_j \\ -p\varepsilon_j & p & -qS_j & qC_j \end{bmatrix} \begin{Bmatrix} A_1 \\ A_2 \\ A_3 \\ A_4 \end{Bmatrix} \tag{11}$$

where the prime denotes differentiation with respect to $\xi_j$, and $\varepsilon_j$, $C_j$, and $S_j$ are defined as follows:

$$\varepsilon_j = \exp(-p\mu_j) \;\; , \;\; C_j = \cos q\mu_j , \;\; S_j = \sin q\mu_j \tag{12}$$

The determinant of the matrix in Eq. (11), denoted $\Delta_j$, is given by

$$\Delta_j = 4pq\varepsilon_j - 2pq(1+\varepsilon_j^2)C_j + \gamma^2(1-\varepsilon_j^2)S_j \tag{13}$$

When $\Delta_j \neq 0$, Eq. (11) can be inverted to solve for the solution coefficients in terms of the end slopes and displacements. Substituting the resulting expressions for the solution

coefficients into Eq. (8) and collecting terms allows the spatial form of the solution $Y(\xi_j)$ to be expressed in terms of end rotations and displacements using nondimensional shape functions as follows:

$$Y(\xi_j) = \alpha_a N_1(\xi_j) + \theta_a l_0 N_2(\xi_j) + \alpha_b N_3(\xi_j) + \theta_b l_0 N_4(\xi_j) \tag{14}$$

where $0 \le \xi_j \le \mu_j$ and it follows from symmetry considerations that $N_1(\xi_j) = N_3(\mu_j - \xi_j)$ and $N_2(\xi_j) = -N_4(\mu_j - \xi_j)$. Expressions for $N_1(\xi_j)$ and $N_2(\xi_j)$ are given in Eqs. (39) and (40) in the Appendix. Eq. (14), combined with the complex exponential time variation in Eq. (7), can then be substituted into the four equilibrium conditions in Eqs. (5) and (6) to obtain the following dynamic stiffness relationship:

$$\frac{EI}{l_0^3}\begin{bmatrix} k_{11}^j & k_{12}^j & k_{13}^j & k_{14}^j \\ k_{12}^j & k_{22}^j & -k_{14}^j & k_{24}^j \\ k_{13}^j & -k_{14}^j & k_{11}^j & -k_{12}^j \\ k_{14}^j & k_{24}^j & -k_{12}^j & k_{22}^j \end{bmatrix} \begin{Bmatrix} \alpha_a \\ \theta_a l_0 \\ \alpha_b \\ \theta_b l_0 \end{Bmatrix} = \begin{Bmatrix} V_a \\ M_a / l_0 \\ V_b \\ M_b / l_0 \end{Bmatrix} \tag{15}$$

in which $e^{i\omega t}$ has been factored from both sides. Explicit expressions for the six unique coefficients in the dynamic stiffness matrix are given in Eqs. (33) - (38) in the Appendix.

### *Characteristic Equations*

In the case of clamped supports, the displacements and rotations are constrained to be zero at both supports, so that the global dynamic stiffness relation is expressed in terms of the displacement and rotation at the damper, denoted $\alpha_c$ and $\theta_c$. Assembling the

dynamic stiffness contributions from the two beam segments into a global stiffness matrix then yields the following equation of dynamic force equilibrium:

$$\frac{EI}{l_0^3}\begin{bmatrix} k_{11}^1 + k_{11}^2 & k_{12}^2 - k_{12}^1 \\ k_{12}^2 - k_{12}^1 & k_{22}^1 + k_{22}^2 \end{bmatrix}\begin{Bmatrix} \alpha_c \\ \theta_c l_0 \end{Bmatrix} = -ci\omega\begin{Bmatrix} \alpha_c \\ 0 \end{Bmatrix} \tag{16}$$

where the right-hand side represents the force in the damper, $F_d(t) = ic\omega\alpha_c e^{i\omega t}$, which is proportional to the velocity at the damper location through the viscous coefficient $c$. Eq. (16) can be written in nondimensional form by introducing the following alternative nondimensional versions of $c$:

$$\hat{c} = \frac{c}{\sqrt{Tm}};\ \tilde{c} = \frac{cl_0}{\sqrt{mEI}} \tag{17}$$

The "taut-string" nondimensionalization $\hat{c}$, suitable for large $\gamma$, and the "beam" nondimensionalization $\tilde{c}$, suitable for small $\gamma$, are related by $\tilde{c} = \gamma\hat{c}$. Using the "beam" nondimensionalization $\tilde{c}$, expressing $\omega$ in terms of *p* and *q* using Eqs. (10) and (2), and moving the term associated with the damping force to the left-hand side, Eq. (16) can be written as

$$\begin{bmatrix} k_{11}^1 + k_{11}^2 + i\tilde{c}pq & k_{12}^2 - k_{12}^1 \\ k_{12}^2 - k_{12}^1 & k_{22}^1 + k_{22}^2 \end{bmatrix}\begin{Bmatrix} \alpha_c \\ \theta_c l_0 \end{Bmatrix} = \begin{Bmatrix} 0 \\ 0 \end{Bmatrix} \tag{18}$$

For nontrivial solutions, the determinant of the matrix in Eq. (18) must equal zero, which yields the following characteristic equation:

$$\left[(k_{11}^1 + k_{11}^2)(k_{22}^1 + k_{22}^2) - (k_{12}^2 - k_{12}^1)^2\right] + i\tilde{c}pq(k_{22}^1 + k_{22}^2) = 0 \tag{19}$$

Multiplying this equation by $\Delta_1\Delta_2$ removes the singularities associated with the zeros of $\Delta_1$ and $\Delta_2$, where $\Delta_j$ is given by Eq. (13). After dividing by $4pq(p^2+q^2)^2$ and

simplifying, the characteristic equation can then be expressed in the following relatively simple form:

$$Q_0^{CC} + i\tilde{c}\,\frac{Q_1^{CC}Q_2^{CP} + Q_1^{CP}Q_2^{CC}}{2(p^2+q^2)} = 0 \tag{20}$$

where $Q_j^{CC}$ and $Q_j^{CP}$ are defined as follows:

$$\begin{aligned} Q_j^{CC} = &\left[\, p(1-\varepsilon_j)\cos\tfrac{1}{2}q\mu_j + q(1+\varepsilon_j)\sin\tfrac{1}{2}q\mu_j \,\right] \\ &\times\left[\, p(1+\varepsilon_j)\sin\tfrac{1}{2}q\mu_j - q(1-\varepsilon_j)\cos\tfrac{1}{2}q\mu_j \,\right] \end{aligned} \tag{21}$$

$$Q_j^{CP} = p(1+\varepsilon_j^2)\sin q\mu_j - q(1-\varepsilon_j^2)\cos q\mu_j \tag{22}$$

The superscript *CC* represents "clamped-clamped", and the zeros of $Q_j^{CC}$ correspond to the eigenfrequencies of the *j*th segment (of nondimensional length $\mu_j$) with both ends clamped. Similarly, the subscript *CP* represents "clamped-pinned", and the zeros of $Q_j^{CP}$ correspond to the eigenfrequencies of the *j*th segment with one end clamped and one end pinned. The subscript $j = 0$ in Eq. (20) denotes the total span, with nondimensional length $\mu_0 = 1$. It is noted that $Q_j^{CC} = \Delta_j / 2$, where $\Delta_j$ is the determinant of the matrix in Eq. (11) and is defined in Eq. (13). The expression for $Q_j^{CC}$ in Eq. (21) has been factored so that the zeros of the first bracketed factor correspond to symmetric modes and the zeros of the second bracketed factor correspond to anti-symmetric modes. It is also noted that $Q_j^{CP} = k_{22}^j \Delta_j / (p^2+q^2)$, where the dynamic stiffness coefficient $k_{22}^j$ is defined in Eq. (37).

In the case of pinned supports, the displacement is constrained to be zero at each pin support, while the rotations at the supports, denoted $\theta_1$ and $\theta_2$, may be nonzero.

Assembling the dynamic stiffness contributions from the two beam segments into a global stiffness matrix and rearranging as in Eq. (18) then yields the following equation:

$$\begin{bmatrix} k_{11}^1 + k_{11}^2 + i\tilde{c}pq & k_{12}^2 - k_{12}^1 & -k_{14}^1 & k_{14}^2 \\ k_{21}^2 - k_{21}^1 & k_{22}^1 + k_{22}^2 & k_{24}^1 & k_{24}^2 \\ -k_{14}^1 & k_{24}^1 & k_{22}^1 & 0 \\ k_{14}^2 & k_{24}^2 & 0 & k_{22}^2 \end{bmatrix} \begin{Bmatrix} \alpha_c \\ \theta_c l_0 \\ \theta_1 l_0 \\ \theta_2 l_0 \end{Bmatrix} = \begin{Bmatrix} 0 \\ 0 \\ 0 \\ 0 \end{Bmatrix} \tag{23}$$

For nontrivial solutions, the determinant of the matrix in Eq. (23) must equal zero, which gives the characteristic equation for this system. As in the clamped-clamped case, multiplying this characteristic equation by $\Delta_1\Delta_2$ removes the singularities associated with the zeros of $\Delta_1$ and $\Delta_2$, and after dividing by $2pq(p^2+q^2)^4$ and simplifying, the characteristic equation can be expressed in the following form:

$$Q_0^{PP} + i\tilde{c}\frac{Q_1^{PP}Q_2^{CP} + Q_1^{CP}Q_2^{PP}}{2(p^2+q^2)} = 0 \tag{24}$$

where $Q_j^{CP}$ is defined in Eq. (22) and $Q_j^{PP}$ is defined as follows:

$$Q_j^{PP} = (1-\varepsilon_j^2)\sin q\mu_j \tag{25}$$

The superscript *PP* represents "pinned-pinned", and the zeros of $Q_j^{PP}$ correspond to the eigenfrequencies of the *j*th segment with both ends pinned. It is noteworthy that the characteristic equations in the cases of clamped and pinned supports, Eqs. (20) and (24), have exactly the same form, with the only difference being that each occurrence of $Q_j^{CC}$ in Eq. (20) is replaced by $Q_j^{PP}$ in Eq. (24). Solution of Eqs. (20) and (24) for the complex eigenfrequencies is discussed in the following main section.

### *Complex Mode Shapes*

The mode shape associated with a given eigenfrequency can be expressed over each segment in terms of the nonzero end displacements and rotations using the frequency-dependent shape functions as in Eq. (14). These shape functions are evaluated at the eigenfrequency corresponding to the mode of interest, and the resulting mode shapes are generally complex-valued, representing variation in the phase of oscillation along the span. In the case of clamped supports, the mode shapes can be expressed in terms of the displacement $\alpha_c$ and the rotation $\theta_c$ at the damper as follows:

$$Y(\xi_1) = \alpha_c N_3(\xi_1) + \theta_c l_0 N_4(\xi_1)\,;\; Y(\xi_2) = \alpha_c N_1(\xi_2) + \theta_c l_0 N_2(\xi_2) \tag{26}$$

where $Y(\xi_1)$ applies for $0 \le \xi_1 \le \mu_1$ and $Y(\xi_2)$ for $0 \le \xi_2 \le \mu_2$. The relationship between $\alpha_c$ and $\theta_c$ for a given mode shape is obtained from the eigenproblem in Eq. (18), and because the matrix in Eq. (18) is rank-deficient when evaluated at an eigenfrequency, the first row can be eliminated to obtain the following relationship:

$$\theta_c l_0 = \alpha_c (k_{12}^1 - k_{12}^2)/(k_{22}^1 + k_{22}^2) \tag{27}$$

where the dynamic stiffness coefficients are evaluated at the eigenfrequency of the specified mode. In the case of pinned supports, the rotations at the supports, $\theta_1$ and $\theta_2$, also enter the expressions for the mode shapes, and the relationship between $\alpha_c$, $\theta_c$, $\theta_1$, and $\theta_2$ for a given mode shape is obtained from the eigenproblem in Eq. (23). Because the matrix in Eq. (23) is rank-deficient when evaluated at an eigenfrequency, the first row can be eliminated to yield three independent equations relating $\alpha_c$, $\theta_c$, $\theta_1$, and $\theta_2$. While the scaling of the complex mode shapes is arbitrary, it is convenient to choose a scaling such that $\alpha_c$ is purely real. This scaling facilitates physical interpretation in cases of

small damping for which the eigenfrequencies are "mostly" real ( $\mathrm{Im}[\omega] \ll \mathrm{Re}[\omega]$ ), as discussed in Main and Jones (2005).

## Complex Eigenfrequencies

### *Limiting Real-Valued Eigenfrequencies*

In considering the solutions to the characteristic Eqs. (20) and (24), it is convenient to begin by considering solutions associated with the limiting cases of undamped ( $\tilde{c} = 0$ ) and fully locked ( $\tilde{c} \to \infty$ ) vibration. In these limiting cases, the eigenfrequencies are real-valued, corresponding to non-decaying oscillations. With $\tilde{c} = 0$, the second terms in Eqs. (20) and (24) vanish, and the characteristic equations reduce to $Q_0^{CC} = 0$ and $Q_0^{PP} = 0$ for clamped and pinned supports, respectively. The solutions of these equations simply correspond to the undamped eigenfrequencies, which are denoted $\omega_{0n}$, where the subscript 0 denotes the undamped system ( $c = 0$ ), and $n$ denotes the mode number. In the limit as $\tilde{c} \to \infty$, the damper acts as an intermediate pin support, constraining the displacement at the damper to zero, but leaving rotations at the damper unrestrained. Dividing Eqs. (20) and (24) by $\tilde{c}$ and taking the limit as $\tilde{c} \to \infty$ eliminates the first terms, and the characteristic equations with an intermediate pin support are given as follows:

$$Q_1^{CC} Q_2^{CP} + Q_1^{CP} Q_2^{CC} = 0 \tag{28}$$

$$Q_1^{PP} Q_2^{CP} + Q_1^{CP} Q_2^{PP} = 0 \tag{29}$$

where Eq. (28) corresponds to clamped ends and Eq. (29) corresponds to pinned ends. The solutions to Eqs. (28) and (29), which must be evaluated numerically, correspond to

the eigenfrequencies of the fully locked systems and are denoted $\omega_{\infty n}$, where the subscript $\infty$ denotes $\tilde{c} \to \infty$ and $n$ is the mode number.

### *Eigenfrequency Loci*

As the damper coefficient $\tilde{c}$ varies between 0 and $\infty$, the complex eigenfrequencies trace loci in the complex plane, which originate at the undamped eigenfrequencies and terminate at the fully locked frequencies. In investigating the form of these loci, it is helpful to rearrange the characteristic Eqs. (20) and (24) to isolate the nondimensional damper coefficient $\tilde{c}$. Noting that $\tilde{c}$ is real-valued, the resulting equations can be separated into real and imaginary parts as follows:

$$\mathrm{Re}\left[\frac{2(p^2+q^2)Q_0^{CC}}{Q_1^{CP}Q_2^{CC}+Q_1^{CC}Q_2^{CP}}\right]=0\,;\ \mathrm{Im}\left[\frac{2(p^2+q^2)Q_0^{CC}}{Q_1^{CP}Q_2^{CC}+Q_1^{CC}Q_2^{CP}}\right]=-\tilde{c} \tag{30}$$

$$\mathrm{Re}\left[\frac{2(p^2+q^2)Q_0^{PP}}{Q_1^{PP}Q_2^{CP}+Q_1^{CP}Q_2^{PP}}\right]=0\,;\ \mathrm{Im}\left[\frac{2(p^2+q^2)Q_0^{PP}}{Q_1^{PP}Q_2^{CP}+Q_1^{CP}Q_2^{PP}}\right]=-\tilde{c} \tag{31}$$

where Eq. (30) corresponds to clamped supports and Eq. (31) corresponds to pinned supports. The real parts of Eqs. (30) and (31), which are independent of $\tilde{c}$, define the loci of all possible values of the eigenfrequencies in the complex plane, for prescribed values of the damper location $\mu_1$ and the bending stiffness parameter $\gamma$. The eigenfrequency loci can be evaluated numerically by incrementing the real part of the complex frequency $\mathrm{Re}[\omega]$ and at each step evaluating the corresponding value(s) of the imaginary part $\mathrm{Im}[\omega]$ for which the real part of Eq. (30) or Eq. (31) is satisfied. As will be observed subsequently, no solutions exist over some ranges of $\mathrm{Re}[\omega]$, while multiple solutions exist over other ranges of $\mathrm{Re}[\omega]$. The value of the damper coefficient $c$ corresponding to

any particular point on the loci can be determined from the imaginary part of Eq. (30) or Eq. (31). This procedure enables an exploration of the solution characteristics for all possible values of the damper coefficient $\tilde{c}$, and it is used subsequently to investigate the influence of damper location. However, when the damper is located relatively near a support and the aim is to determine the complex eigenfrequencies corresponding to a specific value of the damper coefficient $c$, this can be accomplished more efficiently using iterative relations presented in Main and Jones (2005).

### *Overdamped Solutions*

Overdamped solutions correspond to cases for which the eigenfrequency is purely imaginary, being expressible as $\omega = i\sigma$, where $\sigma$ is real and positive. The time variation associated with such solutions is given by $e^{-\sigma t}$, according to the exponential form assumed in Eq. (7), and these solutions are characterized by non-oscillatory decay. Alternative nondimensionalizations of the decay rate can be defined as in Eq. (2): $\hat{\sigma} = \sigma / \omega_{01}^{S}$ and $\tilde{\sigma} = \sigma / \omega_{01}^{B}$. Using Eq. (10), $p$ and $q$ can be expressed in terms of these as follows:

$$\left.\begin{matrix} p \\ q \end{matrix}\right\} = \sqrt{\sqrt{(\tfrac{1}{2}\gamma^2)^2 - (\pi\gamma\hat{\sigma})^2} \pm \tfrac{1}{2}\gamma^2} = \sqrt{\sqrt{(\tfrac{1}{2}\gamma^2)^2 - (\pi^2\tilde{\sigma})^2} \pm \tfrac{1}{2}\gamma^2} \tag{32}$$

Interestingly, it is found that when $p$ and $q$ are given by Eq. (32), the real parts of Eqs. (30) and (31) are automatically satisfied. This can be shown analytically for cases when $\hat{\sigma} < \gamma/(2\pi)$ or $\tilde{\sigma} < \gamma^2/(2\pi^2)$, for which it follows from Eq. (32) that $p^2 > 0$ and $q^2 < 0$, so that $p$ is purely real while $q$ is purely imaginary. When $\hat{\sigma} > \gamma/(2\pi)$ or $\tilde{\sigma} > \gamma^2/(2\pi^2)$, $p$ and $q$ are complex-valued, and while it has not been shown

analytically, calculations using arbitrary precision arithmetic over a wide range of $\gamma$ and $\mu_1$ have demonstrated that the real parts of Eqs. (30) and (31) are satisfied in such cases as well.

It is thus observed that any arbitrary value of $\sigma$ is a solution to the characteristic Eqs. (20) and (24), and the corresponding value of $c$ can be evaluated from the imaginary part of Eq. (30) or Eq. (31), depending on the support conditions. Fig. 3(a) shows a resulting plot of $\hat{\sigma}$ versus $\hat{c}$ for the case of clamped supports with $\gamma = 100$ and a damper location of $\mu_1 = 0.3$. The curve corresponding to the taut-string limit ($\gamma \to \infty$) is also plotted for reference, using the expression in Main and Jones (2002). The mode shapes associated with the points labeled in Fig. 3(a) are plotted in Fig. 3(b). Fig. 3 shows that for both $\gamma = 100$ and $\gamma \to \infty$, non-oscillatory solutions emerge only when the damper coefficient $\hat{c}$ exceeds a critical value. In the taut-string limit, this critical value is given by $\hat{c}^{crit} = 2$, with the decay rate $\hat{\sigma}$ being undefined for $\hat{c} = 2$ and decreasing monotonically with $\hat{c}$ for $\hat{c} > 2$. The point labeled *ii* in Fig. 3(a) corresponds to the case of critical damping for $\gamma = 100$, having the lowest value of $\hat{c}$ for which a non-oscillatory solution exists. In contrast with the taut-string result, the case of critical damping for finite $\gamma$ is associated with a finite value of the decay rate $\hat{\sigma} = \hat{\sigma}^{crit}$, and for $\hat{c} > \hat{c}^{crit}$, two non-oscillatory solutions exist. Along the lower branch of solutions, associated with slower decay, the decay rate $\hat{\sigma}$ decreases monotonically with increasing $\hat{c}$, while the associated mode shape, illustrated for point *iii* in Fig. 3(b), approaches the static deflected shape of the tensioned beam under a concentrated load. Along the upper branch, associated with faster decay, the decay rate $\hat{\sigma}$ increases monotonically with $\hat{c}$, while the associated mode shape, illustrated for point *i* in Fig. 3(b), becomes increasingly localized

about the damper location. For a given supercritical value of the damper coefficient, two non-oscillatory solutions generally exist, as illustrated by points *i* and *iii* in Fig. 3, which both correspond to $\hat{c} = 3$. While $\hat{c}^{crit}$ is independent of the damper location for the taut string, $\hat{c}^{crit}$ is found to decrease with increasing $\mu_1$ for finite values of $\gamma$, reaching its minimum value when $\mu_1 = 0.5$. For a given damper location, $\hat{c}^{crit}$ increases with decreasing $\gamma$.

## "Curve Veering" of Fully Locked Eigenfrequencies

In the limit of zero bending stiffness ($\gamma \to \infty$), previously considered in Main and Jones (2002), vibrations of the two segments on either side of the fully locked damper are uncoupled, and distinct eigenfrequencies are associated with these two segments. The characteristic equation in this limit reduces to $\sin(q\mu_1)\sin(q\mu_2) = 0$, where the zeros of $\sin(q\mu_2)$ correspond to eigenfrequencies of the longer segment, which increase monotonically with $\mu_1$, and the zeros of $\sin(q\mu_1)$ correspond to eigenfrequencies of the shorter segment, which decrease monotonically with increasing $\mu_1$. Crossings of these distinct eigenfrequencies occur when the damper is located at a node of an undamped mode, and at these points, fully locked eigenfrequencies of the two segments coincide with an eigenfrequency of the undamped system. In contrast, finite bending stiffness requires continuity of slope across the damper, which couples the vibrations of the two segments, including the limiting case of a fully locked damper. As a consequence, adjacent eigenfrequencies of the fully locked system no longer cross when the damper passes a node of the undamped system, but instead converge and then veer apart, an

example of the "curve veering" phenomenon discussed by Perkins and Mote (1986). Between veerings, the fully locked eigenfrequencies alternately increase and decrease with increasing $\mu_1$, while vibrations of the longer and shorter segments alternately predominate in the corresponding mode shapes.

These features are illustrated in Fig. 4 for the case of clamped supports with $\gamma = 100$. In Fig. 4(a), the fully locked eigenfrequencies $\hat{\omega}_{\infty n}$ ("taut-string" nondimensionalization) are plotted against the damper location $\mu_1$. The undamped eigenfrequencies $\hat{\omega}_{0n}$, which are independent of the damper location, are also plotted as dashed horizontal lines for reference. The mode shapes corresponding to points labeled on the loci of Fig. 4(a) are shown in Fig. 4(b). On loci segments for which a fully locked eigenfrequency $\hat{\omega}_{\infty n}$ increases with $\mu_1$, the corresponding mode shapes are predominantly associated with vibrations of the longer segment to the right of the damper, as illustrated at points *ii* and *vi* in Fig. 4. On loci segments for which $\hat{\omega}_{\infty n}$ decreases with increasing $\mu_1$, the corresponding mode shapes are predominantly associated with vibrations of the shorter segment to the left of the damper, as illustrated at point *iv* in Fig. 4.

A local maximum for the *n*th fully locked eigenfrequency $\hat{\omega}_{\infty n}$ occurs when the damper is located at a node of undamped mode $n+1$, as illustrated at point *iii* in Fig. 4, where $\hat{\omega}_{\infty 3}$ attains a local maximum as it veers away from $\hat{\omega}_{\infty 4}$. At such local maxima, the eigenfrequency and mode shape of fully locked mode $n$ are equivalent to those of undamped mode $n+1$. A local minimum for $\hat{\omega}_{\infty n}$ occurs when the damper is located slightly past a node of undamped mode $n$, as illustrated at point *v* in Fig. 4, where $\hat{\omega}_{\infty 3}$

attains a local minimum as it veers away from $\hat{\omega}_{\infty 2}$. At such local minima, $\hat{\omega}_{\infty n}$ is somewhat higher than $\hat{\omega}_{0n}$, and the mode shape corresponding to $\hat{\omega}_{\infty n}$ has zero slope at the damper location, with displacement having the same sign on each side of the damper, as illustrated for point *v* in Fig. 4(b). Interestingly, the local maxima such as point *iii* correspond to cases in which $Q_2^{CP} = Q_1^{CP} = 0$, while the local minima such as point *v* correspond to cases in which $Q_2^{CC} = Q_1^{CC} = 0$. In both of these special cases, Eq. (28) is trivially satisfied.

The "curve-veering" phenomenon is illustrated more clearly in Fig. 5(a), which shows a magnification of Fig. 4(a) in the vicinity of point *v*, where point *ii* in Fig. 5(a) corresponds to point *v* in Fig. 4(a). The evolution of the mode shapes corresponding to the veering curves is illustrated in Fig. 5(b) for the points labeled in Fig. 5(a). Perkins and Mote (1986) note that a characteristic of curve-veering is that "the eigenfunctions associated with the eigenvalues on each locus before veering are interchanged during veering in a rapid but continuous way," and this behavior is clearly evident in Fig. 5, where the mode shape associated with point *i*, before veering, closely resembles the mode shape associated with point *vi*, after veering. Similarly, the mode shape associated with point *iv* closely resembles the mode shape associated with point *iii*. As $\gamma$ increases, the minima and maxima of adjacent eigenfrequency loci converge, and the veering becoming increasingly sharp. Finally, in the limit as $\gamma \to \infty$, adjacent maxima and minima touch and crossings of the loci occur rather than veerings. Conversely, as $\gamma$ decreases to zero, the separation between the maxima and minima of adjacent curves increases, and the veerings become more gradual oscillations, as in the eigenfrequency loci for double-span beams without axial load presented by Gorman (1974).

In the case of pinned supports, the fully locked eigenfrequencies and mode shapes exhibit features that are generally similar to those shown for the clamped case in Fig. 4, with the local maxima corresponding to cases in which $Q_2^{PP} = Q_1^{PP} = 0$ and the local minima corresponding to cases in which $Q_2^{CP} = Q_1^{CP} = 0$. However, an important distinction concerns the behavior as the damper approaches a support, $\mu_1 \to 0$. In the case of clamped supports, the fully locked eigenfrequencies approach the undamped eigenfrequencies ($\omega_{\infty n} \to \omega_{0n}$) as $\mu_1 \to 0$, as illustrated at point *i* in Fig. 3. However, in the case of pinned supports, the fully locked eigenfrequencies do not approach the undamped eigenfrequencies as $\mu_1 \to 0$. Rather, as $\mu_1 \to 0$ with pinned supports, locking of the damper effectively transforms the support condition from pinned to clamped, and with finite bending stiffness, the eigenfrequencies associated with clamped-pinned supports are somewhat higher than those associated with pinned-pinned supports. Gorman (1974) previously noted this effect for a double-span beams without axial load ($\gamma = 0$). While the distinction between a clamped and pinned support becomes immaterial as $\gamma \to \infty$, the difference can be important for moderate values of $\gamma$, and it is noted (Main and Jones 2005) that when the damper is located near a support ($\mu_1 \ll 1$), it can produce a much more significant effect with pinned supports than with clamped supports.

## Evolution of Eigenfrequency Loci with Damper Location

### *Damper Between Support and First Node: Three Regimes*

As the damper location $\mu_1$ is varied from a support past the first anti-node to the first node of a given undamped mode shape, the eigenfrequency locus associated with that mode exhibits features corresponding to three distinct regimes, which prevail over different ranges of $\mu_1$. The general features of these three regimes persist over the full range of $\gamma$, from the limit of a taut string ($\gamma \to \infty$), previously discussed by Main and Jones (2002), to the case of a beam without tension ($\gamma = 0$), for which loci are presented in Main (2002). Fig. 6 illustrates the features of these three regimes for the third mode in the case of clamped supports with $\gamma = 100$. In the plots of Fig. 6, the undamped eigenfrequencies, from which the loci originate, are indicated with hollow circles plotted along the real axis, and arrowheads plotted along the loci indicate the direction corresponding to increasing values of the damper coefficient $\hat{c}$. The third-mode loci, which originate at $\hat{\omega}_{03} \simeq 3.08$, are of primary interest in Fig. 6, while the loci of neighboring modes are also plotted to illustrate the interactions that define the boundaries between the different regimes. Each subplot in Fig. 6 includes loci for three different damper locations, which are denoted using distinct arrowheads and differing line thickness, as indicated in the legend.

As $\mu_1$ increases from zero, the eigenfrequency locus for any given mode initially exhibits features corresponding to regime 1, which are illustrated for the third mode in Fig. 6(a). In regime 1, the *n*th eigenfrequency locus terminates on the real axis at $\omega_{\infty n}$, which is somewhat greater than $\omega_{0n}$, from which the locus originates. Between these

limits, the decay rate $\mathrm{Im}[\omega]$ increases to a maximum value and then decreases to zero, while the damped frequency $\mathrm{Re}[\omega]$ increases monotonically with increasing $c$. The width at the base of each locus is $\Delta\omega_{\infty n} = \omega_{\infty n} - \omega_{0n}$, and $\Delta\omega_{\infty n}$ increases with $\mu_1$ within regime 1. For small $\Delta\omega_{\infty n}$, the loci are nearly semi-circular, as is shown in Main and Jones (2005), but as $\Delta\omega_{\infty n}$ increases, the loci become increasingly skewed upwards and to the right, as shown in Fig. 6(a). The upper limit of $\mu_1$ within regime 1 corresponds to the value for which the locus of mode $n$ intersects the locus of mode $n+1$. This value of $\mu_1$ could be computed analytically in the taut-string limit (Main and Jones 2002), but it can only be approximated numerically with nonzero bending stiffness. Fig. 6(a) shows that for $\mu_1 = 0.14252$, the loci of the third and fourth modes are approaching an intersection.

As $\mu_1$ is increased beyond the point of intersection between the loci of modes $n$ and $n+1$, the $n$th eigenfrequency locus exhibits the remarkably different features of regime 2, which are illustrated for the third mode in Fig. 6(b). Regime 2 corresponds to damper locations near the first antinode of the undamped mode shape, and rather than bending downwards to approach the real axis, the eigenfrequency loci arch backwards to intersect the imaginary axis. The point at which a locus intersects the imaginary axis corresponds to the case of critical damping, previously illustrated at point *ii* in Fig. 3. As the damper coefficient is further increased beyond this critical point, the locus diverges into two branches, one extending downward and one extending upward along the imaginary axis in Fig. 6(b), and these branches correspond to the upper and lower branches previously illustrated in Fig. 3. It is thus observed that free oscillation in a

particular mode can be completely suppressed by placing the damper sufficiently near the first antinode of the undamped mode shape and tuning the damper coefficient to a value greater than or equal to the critical value. Interestingly, in the taut-string limit ($\gamma \to \infty$), the loci in regime 2 do not intersect the imaginary axis in the finite part of the complex plane; rather, $\mathrm{Im}[\omega] \to \infty$ and $\mathrm{Re}[\omega]$ approaches a finite limiting value along these loci as $\hat{c} \to \hat{c}^{crit}$, while overdamped solutions emerge along the imaginary axis from $+\infty$ when $\hat{c} > \hat{c}^{crit}$ (Main and Jones 2002). It is thus observed that the influence of bending stiffness brings the point of intersection between these branches into the finite part of the complex plane. The upper limit of $\mu_1$ within regime 2 corresponds to the value for which the locus of mode $n$ intersects the locus of mode $n-1$, and in Fig. 6(b), the loci of the second and third modes are approaching an intersection for $\mu_1 = 0.19723$.

As $\mu_1$ is increased beyond the point of intersection between the loci of modes $n$ and $n-1$, the $n$th eigenfrequency locus exhibits the features of regime 3, which are illustrated for the third mode in Fig. 6(c). In regime 3, the $n$th eigenfrequency locus bends backwards and downwards, terminating on the real axis at $\omega_{\infty n-1}$, the eigenfrequency of fully locked mode $n-1$. Because $\omega_{\infty n-1}$ is somewhat less than $\omega_{0n}$, the damped frequency $\mathrm{Re}[\omega]$ is less than $\omega_{0n}$. As $\mu_1$ increases within regime 3, the limiting frequency $\omega_{\infty n-1}$ approaches $\omega_{0n}$, and the width of the locus decreases. The upper limit of $\mu_1$ within regime 3 corresponds to a damper location at the first node of the $n$th undamped mode shape, for which $\omega_{\infty n-1} = \omega_{\infty n}$, and the locus of mode $n$ shrinks to a single point on the real axis, indicating that no damping can be added to this mode. This

condition corresponds to point *iii* in Fig. 4 and to point *v* in Fig. 5 for the fourth mode and the third mode, respectively.

### *Damper Beyond First Node*

While the three regimes described in the previous section persist for all values of $\gamma$, the subsequent evolution of the eigenfrequency loci, as the damper is moved beyond the first node, differs significantly depending on the value of $\gamma$. In particular, the nature of the subsequent evolution depends on the sharpness of "veering" in the fully locked eigenfrequencies, as previously illustrated in Figs. 4 and 5, because such veering occurs as the damper passes a node of the undamped mode shape. In the case of zero axial force ($\gamma = 0$), the veering of the fully locked eigenfrequencies is quite gradual, and the separation of adjacent loci remains sufficiently large that no further intersections of adjacent loci occur for damper locations beyond the first node (Main 2002). Rather, the *n*th locus continues to terminate at $\omega_{\infty n-1}$ for all values of $\mu_1$ beyond the first node, while the locus alternately expands and contracts as the damper location passes subsequent antinodes and nodes of the undamped mode shape. However, for larger values of $\gamma$, the "veering" can become sufficiently sharp that additional intersections do occur between the loci of adjacent modes, as is illustrated by the loci for $\gamma = 100$ presented in Main (2002). While further discussion of this behavior can be found in Main (2002), a number of interesting features are illustrated in Fig. 7, which shows the third- and fourth-mode eigenfrequency loci for $\gamma = 100$ and $\mu_1 = 0.39$, along with selected mode shapes. For the complex mode shapes shown in Fig. 7(b), the real and imaginary parts are denoted by thick and thin lines, respectively, and the damper location is indicated by hollow circles.

The damper location of $\mu_1 = 0.39$ in Fig. 7 is near the second antinode of the fourth undamped mode shape, as can be seen in the plot of the mode shape associated with point *iv* in Fig. 7(b). Interestingly, it is observed in Fig. 7(a) that for this damper location, the fourth-mode locus arches leftward over the smaller third-mode locus to terminate on the real axis at $\omega_{\infty 2}$ (point *vi*) in the limit as $\hat{c} \to \infty$. Fig. 7(b) shows that the mode shape associated with the limit at point *vi* exhibits predominant vibrations of the shorter segment, to the left of the damper. The termination of the locus on the real axis contrasts with the behavior previously observed for a damper near the first antinode in Fig. 6(b) (regime 2), in which the loci intersected the imaginary axis. It is noted that because the locus does not intersect the imaginary axis in this case, it is not possible to completely suppress free oscillations, as could be achieved with a damper near the first antinode. Large values of the decay rate still can be achieved by appropriate tuning of the damper, but as the damper coefficient becomes large, vibrations of the shorter segment to the left of the damper emerge, with the decay rate tending to zero as $\hat{c} \to \infty$.

The points labeled *ii* and *v* in Fig. 7, which both correspond to $\hat{c} \simeq 2.247$, represent an interesting case in which the damped frequencies of the third and fourth modes coincide ($\mathrm{Re}[\hat{\omega}_3] = \mathrm{Re}[\hat{\omega}_4]$), while their decay rates differ ($\mathrm{Im}[\hat{\omega}_3] < \mathrm{Im}[\hat{\omega}_4]$). For $\hat{c} > 2.247$, the damped frequency of the fourth mode is less than that of the third mode ($\mathrm{Re}[\hat{\omega}_4] < \mathrm{Re}[\hat{\omega}_3]$). It is noted that $\hat{c} = 2.247$ is very close to the critical value $\hat{c}^{crit}$ at which non-oscillatory solutions first emerge. Interestingly, in the taut-string limit ($\gamma \to \infty$) the decay rate associated with this critical value $\hat{c}^{crit}$ tends to infinity ($\mathrm{Im}[\hat{\omega}] \to \infty$), and the fourth-mode locus in Fig. 7(a) diverges into two distinct branches, which do not intersect in the finite part of the complex plane. The right branch originates

at the undamped frequency, and along this branch, $\mathrm{Im}[\hat{\omega}] \to \infty$ as $\hat{c}$ increases from zero to approach $\hat{c}^{crit}$. Solutions along the left branch emerge for $\hat{c} > \hat{c}^{crit}$, and along this branch, $\mathrm{Im}[\hat{\omega}]$ decreases from infinity and approaches zero as $\hat{c} \to \infty$. A detailed analysis of these distinct solution branches for the taut string is presented in Main and Jones (2002). It is thus observed in Fig. 7(a), as previously for regime 2 in Fig. 6(b), that the influence of finite bending stiffness brings the point of intersection between two distinct branches into the finite part of the complex plane to form a single continuous locus.

## Conclusions

Exact analytical solutions have been formulated for the complex eigenmodes associated with free vibrations of tensioned beams with an intermediate viscous damper. The problem has been formulated using the dynamic stiffness method, to enable the present formulation to be readily extended to more complicated assemblages of axially loaded beam segments with intermediate attachments. Characteristic equations have been obtained for the cases of clamped and pinned supports, and these equations have been expressed in a relatively simple form in terms of factors associated with cases of single-span vibration. The eigenfrequencies trace loci in the complex plane that originate at the real-valued undamped eigenfrequencies and terminate at the real-valued fully locked eigenfrequences, in which the damper acts as an intermediate pin support. In investigating the influence of damper location, the eigenfrequencies in the fully locked limit ($c \to \infty$) were first considered, and a "curve veering" phenomenon was observed, in which adjacent eigenfrequencies approach and then veer apart as the fully locked damper

passed a node of an undamped mode shape, and an interchange of the mode shapes associated with the veering curves was observed. The veering was found to become sharper as bending stiffness tended to zero, and in the taut-string limit, the fully locked eigenfrequencies cross rather than veering. The evolution of the eigenfrequency loci with varying damper location was then considered, and three distinct regimes of behavior for the loci were identified. The general features of these three regimes were found to persist from the taut-string limit to the case of a beam without tension. The second of the three regimes corresponds to damper locations near the first anti-node of a given undamped mode shape, and in this regime the loci were observed to bend backwards to approach the imaginary axis as the damper coefficient approached a critical value $c \to c^{crit}$. When $c > c^{crit}$, two distinct overdamped solutions emerge, associated with non-oscillatory decay. It is thus observed that by appropriate placement and tuning of the damper, free oscillations of a particular mode of vibration can be completely suppressed. Interestingly, it was observed that for damper locations near subsequent anti-nodes of a given mode, that mode cannot be transformed to a non-oscillatory solution, as could be achieved near the first anti-node. Rather, as $c$ becomes large with the damper near a higher-order antinode, vibrations of the shorter segment, to one side of the damper, become predominant, and the associated decay rate tends to zero as $c \to \infty$.

## Appendix

The six unique coefficients in the dynamic stiffness matrix of Eq. (15) are defined as follows:

$$k_{11}^{j} = pq(p^2+q^2)[(1+\varepsilon_j^2)qS_j + (1-\varepsilon_j^2)pC_j]/\Delta_j \tag{33}$$

$$k_{12}^{j} = pq[-2\gamma^2\varepsilon_j + 2(1-\varepsilon_j^2)pqS_j + \gamma^2(1+\varepsilon_j^2)C_j]/\Delta_j \tag{34}$$

$$k_{13}^{j} = pq(p^2+q^2)[-(1-\varepsilon_j^2)p - 2q\varepsilon_j S_j]/\Delta_j \tag{35}$$

$$k_{14}^{j} = pq(p^2+q^2)[(1+\varepsilon_j^2) - 2\varepsilon_j C_j]/\Delta_j \tag{36}$$

$$k_{22}^{j} = (p^2+q^2)[p(1+\varepsilon_j^2)S_j - q(1-\varepsilon_j^2)C_j]/\Delta_j \tag{37}$$

$$k_{24}^{j} = (p^2+q^2)[q(1-\varepsilon_j^2) - 2p\varepsilon_j S_j]/\Delta_j \tag{38}$$

where $\varepsilon_j$, $C_j$, and $S_j$ are defined in Eq. (12), and $\Delta_j$ is defined in Eq. (13). The nondimensional displacement shape functions in Eq. (14), used to express the spatial form of the solution in terms of the end displacements and slopes, are given by

$$N_1(\xi_j) = a_1^j e^{-p\xi_j} + a_2^j e^{-p(\mu_j-\xi_j)} + a_3^j \cos q\xi_j + a_4^j \sin q\xi_j \tag{39}$$

$$N_2(\xi_j) = b_1^j e^{-p\xi_j} + b_2^j e^{-p(\mu_j-\xi_j)} + b_3^j \cos q\xi_j + b_4^j \sin q\xi_j \tag{40}$$

where the coefficients in Eqs. (39) and (40) are defined as

$$a_1^j = [pq\varepsilon_j - q^2 S_j - pqC_j]/\Delta_j \tag{41}$$

$$a_2^j = [pq + \varepsilon_j(q^2 S_j - pqC_j)]/\Delta_j \tag{42}$$

$$a_3^j = [2pq\varepsilon_j + (1-\varepsilon_j^2)p^2 S_j - pq(1+\varepsilon_j^2)C_j]/\Delta_j \tag{43}$$

$$a_4^j = [-pq(1+\varepsilon_j^2)S_j - (1-\varepsilon_j^2)p^2 C_j]/\Delta_j \tag{44}$$

$$b_1^j = [-q\varepsilon_j - pS_j + qC_j]/\Delta_j \tag{45}$$

$$b_2^j = [q - \varepsilon_j (pS_j + qC_j)] / \Delta_j \tag{46}$$

$$b_3^j = [p(1+\varepsilon_j^2)S_j - q(1-\varepsilon_j^2)C_j] / \Delta_j \tag{47}$$

$$b_4^j = [2p\varepsilon_j - q(1-\varepsilon_j^2)S_j - p(1+\varepsilon_j^2)C_j] / \Delta_j \tag{48}$$

## References


Bergman, L.A. and Hyatt, J.E. (1989). "Green functions for transversely vibrating uniform Euler-Bernoulli beams subject to constant axial preload." *J. Sound Vib.*, 134(1), 175-180.

Bokaian, A. (1990). "Natural frequencies of beams under tensile axial loads." *J. Sound Vib.*, 142, 481-498.

Cole, J.D. (1968). *Perturbation Methods in Applied Mathematics*, Blaisdell, Waltham, Massachusetts.

Clough, R.W. and Penzien, J. (1975). *Dynamics of Structures*. McGraw-Hill, New York, 1975.

Currie, I.G. and Cleghorn, W.L. (1988). "Free lateral vibrations of a beam under tension with a concentrated mass at the midpoint." *J. Sound Vib.*, 123(1), 55-61.

Franklin, P. (1989). "Modal analysis of long systems: a transfer matrix approach." Master's essay, Johns Hopkins University, Baltimore, MD.

Gorman, D.F. (1974). "Free lateral vibration analysis of double-span uniform beams." *Int. J. Mech. Sciences*, 16, 345-351.

Hull, A.J. (1994). "A closed form solution of a longitudinal bar with a viscous boundary condition." *J. Sound Vib.*, 169(1), 19-28.

Irvine, M. (1981). *Cable Structures*, The MIT Press, Cambridge, MA, reprinted 1992, Dover, New York.

Krenk, S. (2000). "Vibrations of a taut cable with an external damper." *J. Applied Mech.*, 67, 772-776.

Krenk, S. (2004). "Complex modes and frequencies in damped structural vibrations." *J. Sound Vib.*, 270, 981-996.

Krenk, S. and Nielsen, S.R.K. (2002). "Vibrations of a shallow cable with a viscous damper." *Proceedings of the Royal Society, London, Series A*, 458, 339-357.

Liu, X.Q., Ertekin, R.C., and Riggs, H.R. (1996). "Vibration of a free-free beam under tensile axial loads." *J. Sound Vib.*, 190(2), 273-282.

Main, J.A. (2002). "Modeling the vibrations of a stay cable with attached damper." PhD. Thesis, Johns Hopkins University.

Main, J.A. and Jones, N.P. (2001). "Evaluation of viscous dampers for stay-cable vibration mitigation." *J. Bridge Eng*., 6(6), 385-397.

Main, J.A. and Jones, N.P. (2002). "Free vibrations of taut cable with attached damper. I: Linear viscous damper." *J. Eng. Mech.*, 128(10), 1062-1071.

Main, J.A. and Jones, N.P. (2005). "Vibration of tensioned beams with intermediate damper. II: Damper near a support." *J. Eng. Mech.*, (in press).

McBride, E.J. (1943). "The free lateral vibrations of a cantilever beam with a terminal dashpot." *J. Applied Mech.*, A168-A172.

Oliveto, G., Santini, A., and Tripodi, E. (1997). "Complex modal analysis of a flexural vibrating beam with viscous end conditions." *J. Sound Vib.*, 200, 327-345.

Pacheco, B.M., Fujino, Y., and Sulekh, A. (1993). "Estimation curve for modal damping in stay cables with viscous damper." *J. Struct. Eng*., ASCE, 119(6), 1961-1979.

Perkins, N.C. and Mote, C.D. (1986). "Comments on curve veering in eigenvalue problems." *J. Sound Vib*., 106, 451-463.

Preumont, A. (2002). *Vibration Control of Active Structures*, 2nd Ed. Kluwer, Dordrecht, The Netherlands.

Rasmussen, E. (1997). "Dampers hold sway." *Civil Engineering Magazine*, 67(3), 40-43.

Singh, R., Lyons, W.M., and Prater, G. (1989). "Complex eigensolution for longitudinally vibrating bars with a viscously damped boundary." *J. Sound Vib.*, 133(2), 364-367.

Seebeck, A. (1852). "Über die querschwingungen gespannter und nicht gespannter elastischer stäbe." *Abhandlungen der Mathematisch-Physischen Class der Königlich Sächsischen Gesellschaft der Wissenschaften*, 131-168.

Tabatabai, H. and Mehrabi, A.B. (2000). "Design of mechanical viscous dampers for stay cables." *J. Bridge Eng.*, ASCE, 5(2), 114-123.

Tang, Y. (2003). "Numerical evaluation of uniform beam modes." *J. Eng. Mech.*, 129(12), 1475-1477.

Wittrick, W.H. (1986). "On the vibration of stretched strings with clamped ends and non-zero flexural rigidity." *J. Sound Vib.*, 110, 79-85.

## Figures

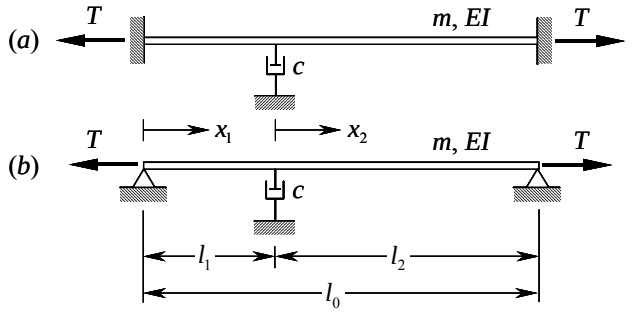


Fig. 1. Tensioned beams with intermediate damper. (a) Clamped supports; (b) Pinned supports.

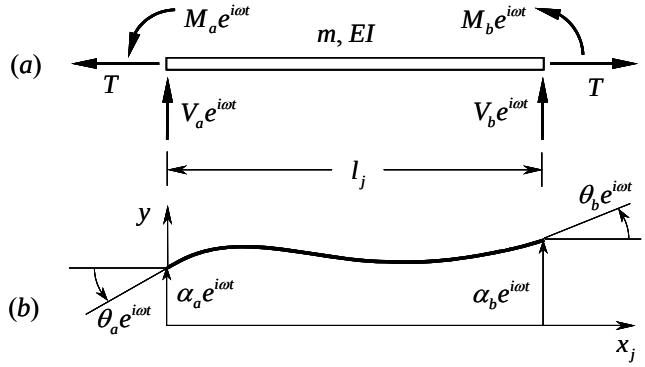


Fig. 2. Tensioned beam segment. (a) End forces; (b) End displacements.

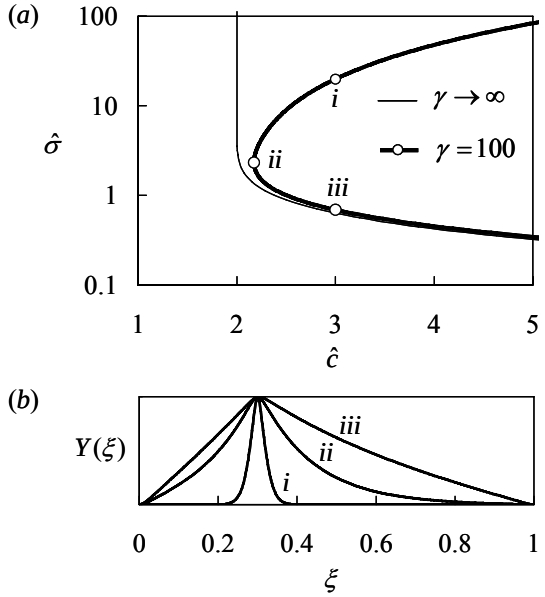


Fig. 3. Overdamped solutions ( $\mu_1 = 0.3$ ). (a) Nondimensional decay rate versus damper coefficient; (b) Corresponding mode shapes for $\gamma = 100$ .

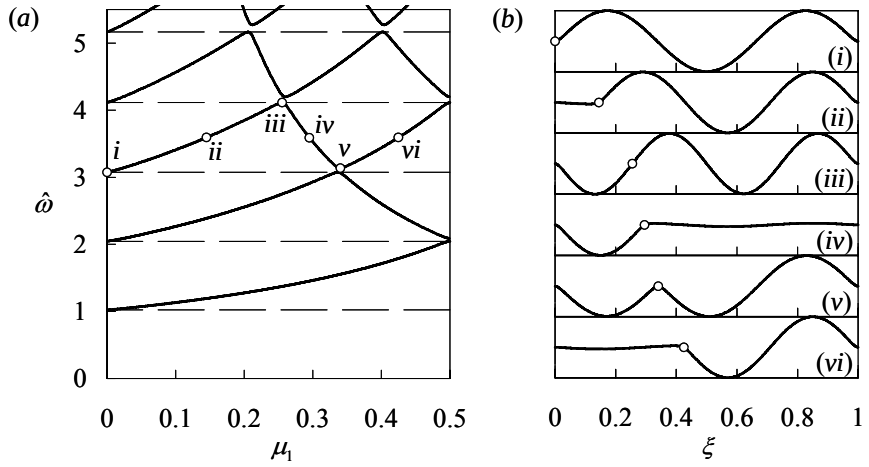


Fig. 4. Influence of damper location $\mu_1$ on (a) eigenfrequencies and (b) mode shapes of system with fully locked damper $c \to \infty$. ($\gamma = 100$)

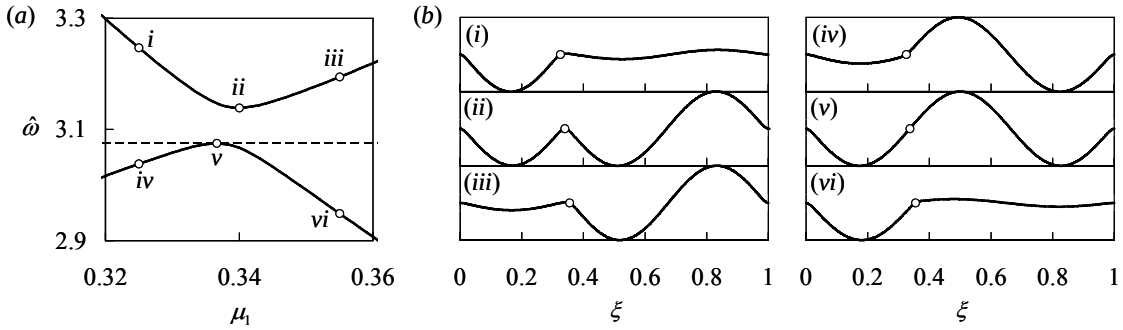


Fig. 5. (a) "Curve veering" of fully locked eigenfrequencies; (b) Corresponding interchange of mode shapes. ($\gamma = 100$)

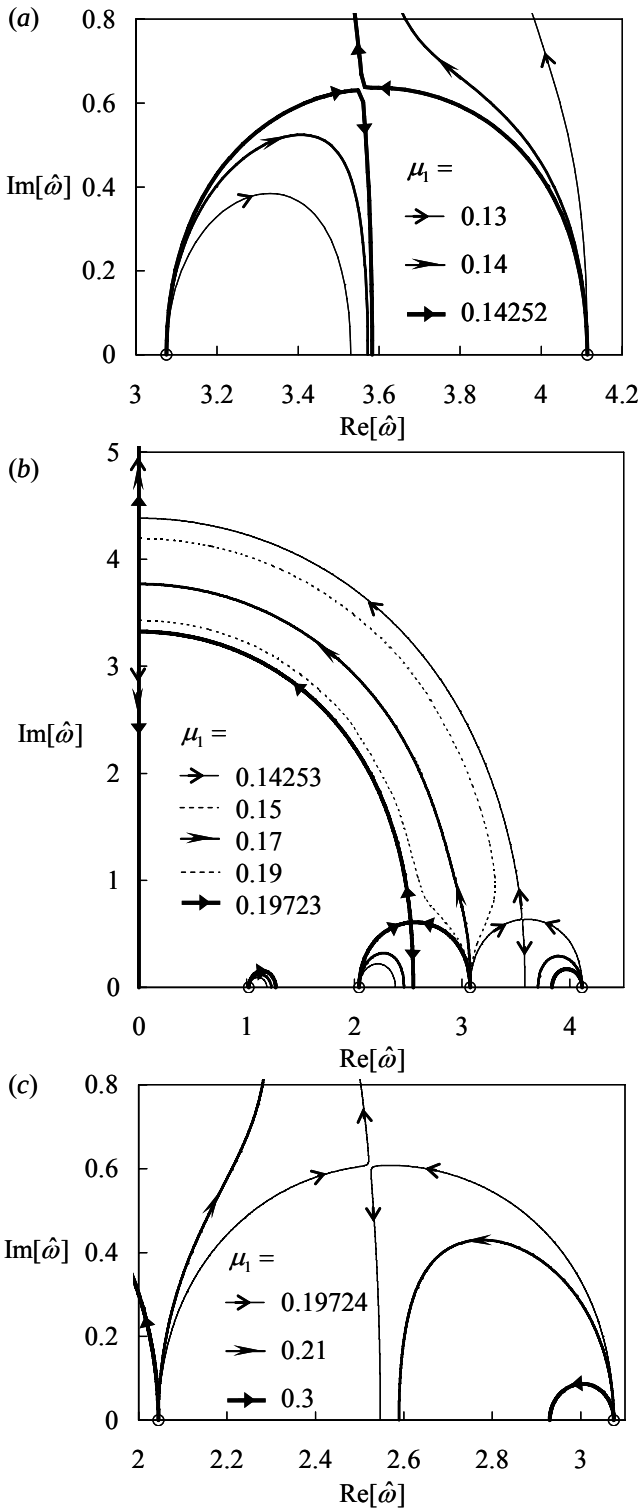


Fig. 6. Eigenfrequency loci as $c$ goes from 0 to $\infty$ (arrows indicate increasing $c$) for different damper locations $\mu_1$ between support and first node. Three regimes are illustrated for the third-mode locus: (a) Regime 1; (b) Regime 2; (c) Regime 3. ($\gamma = 100$)

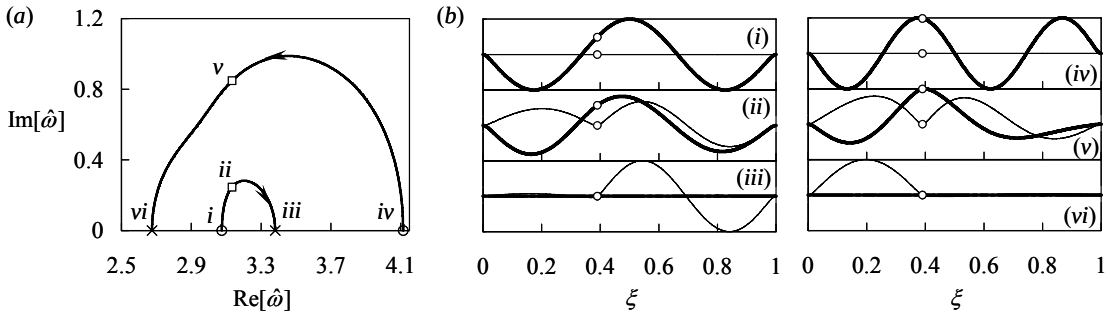


Fig. 7. (a) Third-mode (inner) and fourth-mode (outer) eigenfrequency loci as $c$ goes from 0 to $\infty$ (arrows indicate increasing $c$) for $\mu_1 = 0.39$; (b) Corresponding complex mode shapes: real part ▬, imaginary part ┄, damper location ○. ($\gamma = 100$)